Temporal and thermal evolutions of surface Sr-segregation in pristine and atomic layer deposition modified $La_{0.6}Sr_{0.4}CoO_{3-\delta}$ epitaxial films

Yeting Wen, [a] Tianrang Yang, [a] Dongkyu Lee, [ab] Ho Nyung Lee, [b] Ethan J. Crumlin [c] and Kevin Huang *[a]

The bulk-to-surface Sr segregation can seriously compromise the stability of oxygen electrocatalysis in $La_{1-x}Sr_xCoO_{3-\delta}$ and limit its practical applications such as in solid oxide fuel cells. Here we show *via in situ* ambient pressure X-ray photoelectron spectroscopy (APXPS) that the surface Sr-segregation is a kinetically fast process and the equilibrium surface Sr-concentration follows Arrhenius law from 250 to 520 °C at a fixed $p_{O_2} = 1 \times 10^{-3}$ atm. We also show that application of a nanoscaled, atomic layer deposition (ALD) derived ZrO_2 overcoat can effectively suppress the Sr-segregation by reducing the surface concentration of oxygen vacancies. Electrochemical impedance spectroscopy (EIS) study further confirms that the ALD-ZrO_2-coated LSCo epitaxial film exhibits a much lower and more stable polarization resistance than the uncoated one at 550 °C for >300 hours, suggesting that Sr-segregation is the source of the higher resistance.

1. Introduction

Lanthanum strontium cobaltite $La_{1-x}Sr_xCoO_{3-\delta}$ (LSCo) is an oxygen-deficient, perovskite-structured oxide with high mixed electronic/oxide-ionic conductivity and high oxygen reduction reaction (ORR) activity. Therefore, it is well suited for being a cathode material to work in the intermediate temperature (IT) range, where cathodic ORR kinetics limits the performance of solid oxide fuel cells (SOFCs).[1–4] However, one of the major issues associated with $La_{1-x}Sr_xCoO_{3-\delta}$ is the strong bulk-to-surface Sr-segregation at elevated temperatures. The main compositions of the segregated Sr-rich phase identified so far are insulating SrO, $SrCO_3$ and/or $Sr(OH)_2$,[5–7] a coverage of which rapidly diminishes the original high ORR activity stemming from the strong O-2p and Co-3d orbital covalent mixing, causing performance decay.[8–11] Such chemical and thermal instability has severely limited practical applications of those highly ORR active Sr-doped perovskite cobaltites in IT-SOFCs.

Although the exact driving force for the Sr-segregation is still under investigation, some early studies have shown that elastic and electrostatic interactions between Sr and the lattice are the two major mechanisms for the Sr-segregation.[12,13] Specifically, the electrostatic force is related to the charged defect interactions between the positively charged oxygen vacancy $V_O^{\cdot\cdot}$ and the negatively charged dopant Sr'_{La}. Normally, the surface (and subsurface) concentration of $V_O^{\cdot\cdot}$ for oxygen-deficient perovskites is high, thus forming a positively charged skin to attract the negatively charged dopant Sr'_{La} to the surface.[14] Fister *et al.*[15] confirmed this mechanism with total reflection X-ray fluorescence (TXRF) technique, by which the Sr surface concentration of $La_{0.7}Sr_{0.3}MnO_3$ under different oxygen partial pressures (p_{O_2}) was probed. The Sr-segregation was indeed found to increase with decreasing p_{O_2}. On the other hand, the elastic force introduced by the size mismatch between the dopant and host cations has also been proposed as a driving force for Sr-segregation. For the case of $La_{1-x}Sr_xCoO_{3-\delta}$, the ionic radius of Sr^{2+} (144 pm, CN = 12) is larger than that of La^{3+} (136 pm, CN = 12)[16] so that the dopant Sr^{2+} ions are under compressive stress when substituting on the La-site and could be driven to the surface under much less stress. Lee *et al.*[12] studied the lattice strain effect on the surface cation segregation; the lattice strain were created by doping Ba^{2+} (161 pm, CN = 12), Sr^{2+} (144 pm, CN = 12) and Ca^{2+} (134 pm, CN = 12) into the host La^{3+} in $LaMnO_3$. The authors found that the larger dopants Ba^{2+} and Sr^{2+} would result in more cation rearrangements leading to surface segregation, while the closer dopant Ca^{2+} would have a relatively less surface segregation. By lowering p_{O_2}, the authors also managed to ease the lattice under compressive stress by chemical expansion and observed a reduced surface segregation. However, this finding is contradictory to the electrostatic attraction mechanism that suggests a stronger surface Sr-

[a]*Department of Mechanical Engineering, University of South Carolina, Columbia, South Carolina 29201, USA. E-mail: huang46@cec.sc.edu*

[b]*Materials Sciences and Technology Division, Oak Ridge National Laboratory, Oak Ridge, Tennessee 37831, USA*

[c]*Advanced Light Source, Lawrence Berkeley National Laboratory, Berkeley, California 94720, USA*

segregation under lower p_{O_2}. The controversy may be related to the fact that the compressive stress could be relieved at higher temperatures regardless of cation size mismatch, thus making oxygen stoichiometry the major factor influencing the Sr-segregation.

To mitigate the Sr-segregation and enhance long-term performance stability, Gong *et al.*[17] first demonstrated by overcoating a conformal nanoscale ZrO_2 layer *via* atomic layer deposition (ALD) on $La_{1-x}Sr_xCoO_{3-\delta}$ nanoparticles (NPs) that the original high ORR activity of LSCo NPs can be effectively retained for 4000 h at 700 °C. The authors proposed that the porosity in the ALD-ZrO_2 layer, interdiffusion between Zr and Co and confine-ment of NPs coarsening are the three leading reasons for the ORR activity retention. The authors particularly argued that the interdiffusion-induced substitution of Zr into Co-site has led to

the creation of point defect $Zr^{\bullet}_{Co}$, which can decrease the concentration of surface oxygen vacancies $V^{\bullet\bullet}_{O}$ required by the charge neutrality, thus reducing the electrostatic driving force for Sr'_{La} migration towards surface. In a recent study, Tsvetkov *et al.*[18] further confirmed the idea that a fixed, higher-valent and less reducible cation such as Hf^{4+} and Zr^{4+} can suppress Sr'_{La} migration in LSCo by reducing the concentration of surface $V^{\bullet\bullet}_{O}$, thus the driving force to attract Sr'_{La}. By modifying the surface of $La_{0.8}Sr_{0.2}CoO_{3-\delta}$ epitaxial thin films grown on YSZ single crystal substrates with less reducible oxides derived from metal chloride solutions, the authors showed reduced surface Sr-concentration with improved electrochemical stability.

While the Sr-segregation in $La_{1-x}Sr_xCoO_{3-\delta}$ epitaxial films has been actively studied in recent years, quantification of Sr-segregation process *vs.* temperature and time, particularly under real-world conditions, is rare in the literature. Therefore, the aim of the present study is to investigate how the temperature, time and surface coating affect the surface concentration of Sr in a $La_{1-x}Sr_xCoO_{3-\delta}$ epitaxial film. The tool to attain the surface Sr-concentration is a cutting-edge surface analysis technique, *in situ* synchrotron-based ambient pressure XPS (APXPS).[19] To precisely control the thickness and chemistry of the surface coating, atomic layer deposition (ALD) is applied to make a nanoscaled ZrO_2 layer over the $La_{1-x}Sr_xCoO_{3-\delta}$ epitaxial films. We expect that epitaxial thin films with ALD-overcoat will provide a well-defined platform for in-depth fundamental understanding of surface chemistry without the interference from structural and kinetic complexities encountered in porous and polycrystalline samples.[20] To complement the understanding of APXPS results, electrochemical impedance spectroscopy (EIS) has also been performed on the sister samples under similar conditions for hundreds of hours.

2. Experimental methods

The epitaxial $La_{0.6}Sr_{0.4}CoO_{3-\delta}$ (LSCo) thin films in a thickness of 50 nm were grown on (001)-oriented YSZ by pulsed laser deposition (PLD). Single crystal 9.5 mol% YSZ wafers with the (001) cubic orientation and dimensions of 10 × 5 × 0.5 mm (MTI corporation, USA) were used as the substrate. To prevent the formation of $La_2Zr_2O_7$ [21] at the interface, a layer of 5 nm thick Gd-doped CeO_2 (GDC) buffer layer was also deposited by PLD between YSZ single crystal and LSCo epitaxial film.[22] The YSZ substrate was affixed to the PLD substrate holder using a small amount of silver paint for thermal contact. PLD was performed using a KrF excimer laser at $\lambda = 248$ nm, 10 Hz pulse rate, and 50 mJ pulse energy under a p_{O_2} of 6.6×10^{-5} atm (50 mTorr). For GDC film, a total of 500 pulses was applied to YSZ single crystal substrate at 550 °C, and for LSCo film, a total of 5000 pulses was applied to GDC/YSZ-substrate at 650 °C. After completing the LSCo film deposition, the samples were cooled down to room temperature (RT) in the PLD chamber in ~1 h under the same p_{O_2}.

A precise 0.8 nm thick ZrO_2 layer was further coated on top of the PLD-grown LSCo epitaxial film by ALD in a flow-type reactor (Ultratech Savannah 200 series). Tetrakis(dimethylamido)zirconium(IV) (electronic grade, ≥99.99%, Sigma-Aldrich) and deionized (DI) water were used as Zr-precursor and oxidant, respectively. The reactor temperature was controlled at 180 °C. For a typical cycle, the reactor chamber was first pumped down to 50 mTorr, and then the Zr-precursor was introduced into the chamber by a 0.4 s pulse and stayed for 20 s to completely cover the surface of the sample. Then, a pure N_2 gas at a flow rate of 15 sccm was introduced into the chamber to purge out the residual Zr-precursor. The chamber was then pumped down to 50 mTorr again, followed by a 0.015 s pulse of DI water and holding for 20 s to oxidize the precursor. A typical cycle can be summarized as: pump down → Zr-precursor pulse → N_2 purge → pump down → water pulse → N_2 purge → pump down. The predetermined deposition rate is 0.1 nm per cycle for ALD-ZrO_2, which requires 8 cycles to yield a 0.8 nm thick layer of ZrO_2.

Oxide phase purity and orientation of the deposited thin films were investigated *via* high resolution X-ray diffraction (HRXRD) using a four-circle diffractometer. Measurements were performed in normal and off-normal configurations. The in-plane *a* lattice parameters of LSCo were determined from the off-normal $(202)_{pc}$ peak position (where "pc" denotes the pseudocubic) and the out-of-plane *c* lattice parameters were determined from the $(002)_{pc}$ peak position. Details of lattice parameter calculations can be found elsewhere.[23–25] The surface morphology and roughness of the films synthesized was also checked by atomic force microscopy (AFM, XE-100, PARK System) under a non-contact mode.

The *in situ* APXPS spectra were collected at Beamline 9.3.2 of Advanced Light Source at Lawrence Berkeley National Laboratory.[26] The sample was first placed on a heater on which a thermocouple was attached to measure the temperature. One set of the pristine and overcoated samples were used to investigate the temporal evolution of surface Sr as the temperature was raised from 25 to 520 °C. The heating rate was controlled at 3–5 °C per minute, and there was a holding period of roughly 3 h at 200, 350, 450 and 520 °C under a constant oxygen partial pressure of 1×10^{-3} atm. The spectra collection started with two survey scans (BE = 10–590 eV) at a photon energy of 690 and 695 eV to remove the Auger peaks and continued with low-resolution scans of Sr 3d and La 4d spectra in every 3 min during the entire heating process to capture the fast-changing surface Sr-concentration.

Another set of samples was used to study the isothermal equilibrium concentration of specific element at temperatures

of 25, 250, 350, 450 and 520 °C under oxygen partial pressure of 1×10^{-3} atm. A 30 min hold was given at each temperature before data collection. The data collection began with two survey scans (BE = 10–590 eV) at a photon energy of 690 and 695 eV, followed by a high-resolution scan of Sr 3d, O 1s, La 4d, Co 2p and particularly Zr 3d for the coated sample at a photon energy of 690 eV. The inelastic mean free path (IMFP) of photoelectrons in this measurement was about 1 nm,[27] which becomes the assumed probe depth for this study. The photon energy change in survey scans may cause a shift of peak position in the following scans. So we used La 4d peak as a calibration standard in the analysis. CasaXPS software was used to analyze and deconvolute the spectra.

The electrochemical impedance spectroscopy (EIS) was employed to measure the ohmic and polarization resistances of Ag/LSCo/GDC/YSZ/Ag and Ag/ZrO_2/LSCo/GDC/YSZ/Ag half-cells (GDC: $Gd_{0.2}Ce_{0.8}O_{2-\delta}$) using an electrochemical workstation (Solartron 1255/1287 system) at 550 °C in ambient air as a func-tion of time. To avoid experimental variability, the two cells were loaded side-by-side in the same furnace and EIS measurements were taken sequentially. The sweeping frequency range was varied from 10^6 to 0.005 Hz with an AC stimulus amplitude of 10 mV. The cell configuration is shown in Fig. S1 of the ESI.† Both sides of the sample were covered with silver paste (C8829, Her-aeus) and silver mesh as current collector. The equivalent circuit method in ZSimDemo software was used to extract the resistance values from the collected Nyquist plots.

3. Results and discussion

3.1 Thin film HRXRD patterns

The HRXRD θ–2θ patterns collected at RT are shown in Fig. 1a, where only (00l) (l is integer) peaks of LSCo, GDC, and YSZ can be seen, implying that the LSCo films were grown epitaxially with the (001) orientation of the single-crystal YSZ substrate: $(001)_{pc}$LSCo//$(001)_{cubic}$GDC//$(001)_{cubic}$YSZ. With the 0.8 nm thick ZrO_2 overcoat, no discernible change in the XRD pattern of LSCo was observed. Off-normal Φ scan analysis of the multilayer with and without ZrO_2 overcoat shown in Fig. 1b reveals only {202} plane family for LSCo, GDC and YSZ layers, suggesting a 4-fold cubic symmetry and a cube-on-cube alignment of GDC on YSZ and 45° in-plane rotation of LSCo on GDC. Like previous studies,[23–25] the relaxed lattice parameters, $\hat{a}$ of the epitaxial LSCo films with and without ZrO_2 overcoat obtained in this study vary slightly in the range of 3.828–3.831 Å. This observation implies that a very thin ZrO_2 layer has no influence on in-plane and out-of-plane strains of the LSCo thin film underneath. Therefore, we can ignore the strain effect of ZrO_2 overcoat on the LSCo film.

3.2 Surface morphology of epitaxial films

The surface morphologies of pristine and coated samples after APXPS experiments are examined by AFM and shown in Fig. 2. Some "humps or islands" with a height of ~10 nm are apparent on the surface of the pristine sample after APXPS testing. Given the fact that Sr-enriched particles have been previously observed on the surface of the epitaxial $La_{0.8}Sr_{0.2}CoO_{3-\delta}$ thin films after annealing at 550 °C for 6 h,[24,28,29] it is reasonable to assert that these "islands" are associated with segregated Sr phases. On the contrary, the ALD-ZrO_2 coated sample after APXPS testing shows a much flatter and smoother surface with no obviously large "islands" on the surface, suggesting that the growth of surface Sr-phase has been suppressed by the ZrO_2 overcoat.

3.3 *In situ* APXPS analysis

Time-dependent surface Sr-concentration. The low-resolution Sr 3d and La 4d spectra of the first set of pristine

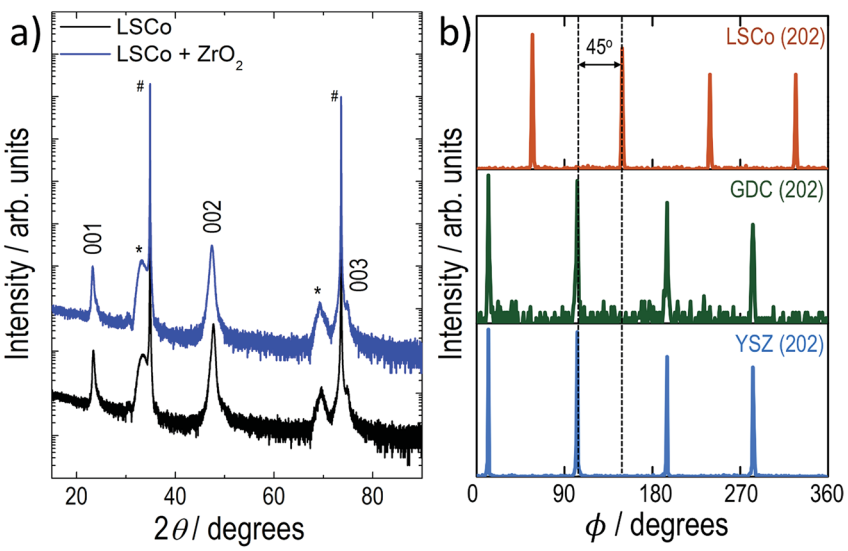

Fig. 1 High resolution X-ray diffraction analysis at RT. (a) Normal XRD of the epitaxial LSCo thin film (black) and LSCo film coated with ZrO_2 (blue). GDC and YSZ substrate peaks are indicated with * and #, respectively. (b) Off-normal XRD of the (202) reflection of a YSZ substrate (light blue), a GDC buffer layer (green), and the (202) reflection of a LSCo thin film (red), confirming the cube-on-cube alignment of GDC on YSZ and 45° in-plane rotation of LSCo on GDC.

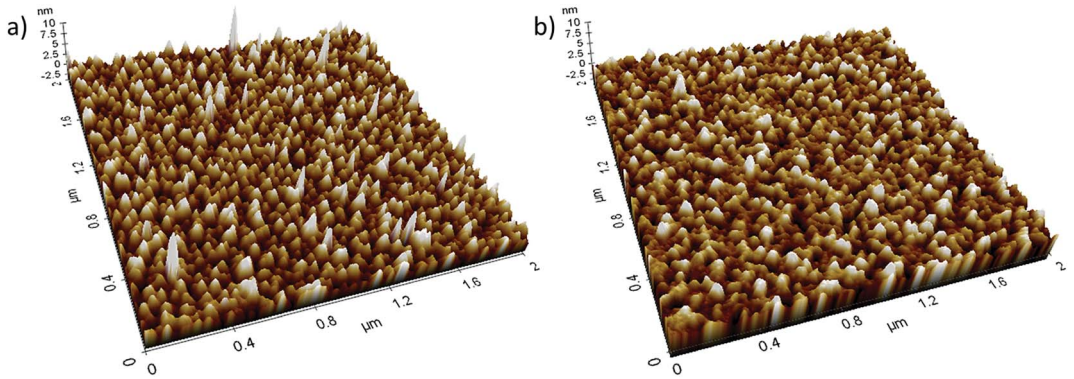

Fig. 2 AFM images of (a) pristine and (b) coated sample after APXPS test.

and ALD-coated LSCo films were collected in every 3 min within a temperature range of 25 to 520 °C at a fixed oxygen partial pressure of 1×10^{-3} atm. The Sr 3d spectra were used to determine the time needed to reach equilibrium concentration at each selected temperature. The La 4d spectra were used to ensure a proper compensation of unstable beam energy and to calibrate the peak positions. This correction sometimes makes binding energies of the same element slightly different in pristine and coated samples or at different temperatures.

In general, the Sr 3d peaks can be divided into 2 sets of Sr $3d_{5/2}$ and $3d_{3/2}$ doublets that belong to surface and lattice Sr.[27] The lower-energy set of Sr 3d is assigned to lattice Sr, whereas the higher set can be assigned to surface Sr that is associated with SrO and $Sr(OH)_2$. The presence of $SrCO_3$ phase can be ruled out because of the lack of C 1s peak when the temperature was above 250 °C. The time-dependent Sr 3d spectra of both samples under 350 °C are shown in Fig. 3a and b as an example. The shape of the spectra remains almost unchanged from 0 to 0.6 h after the temperature was increased to 350 °C. The obtained peak area ratios of the surface Sr (we here used peak area ratio instead of atomic fraction to illustrate the trending because of low-resolution data. We will present more accurate compositions in atomic fractions when dealing with equilibrium concentration later) are further shown as a function of time in Fig. 3c and d for pristine and coated samples, respectively. Note that only data points collected above 200 °C are presented due to the concerns of surface C-species absorptions at low temperatures. It is obvious that the surface Sr area ratio of

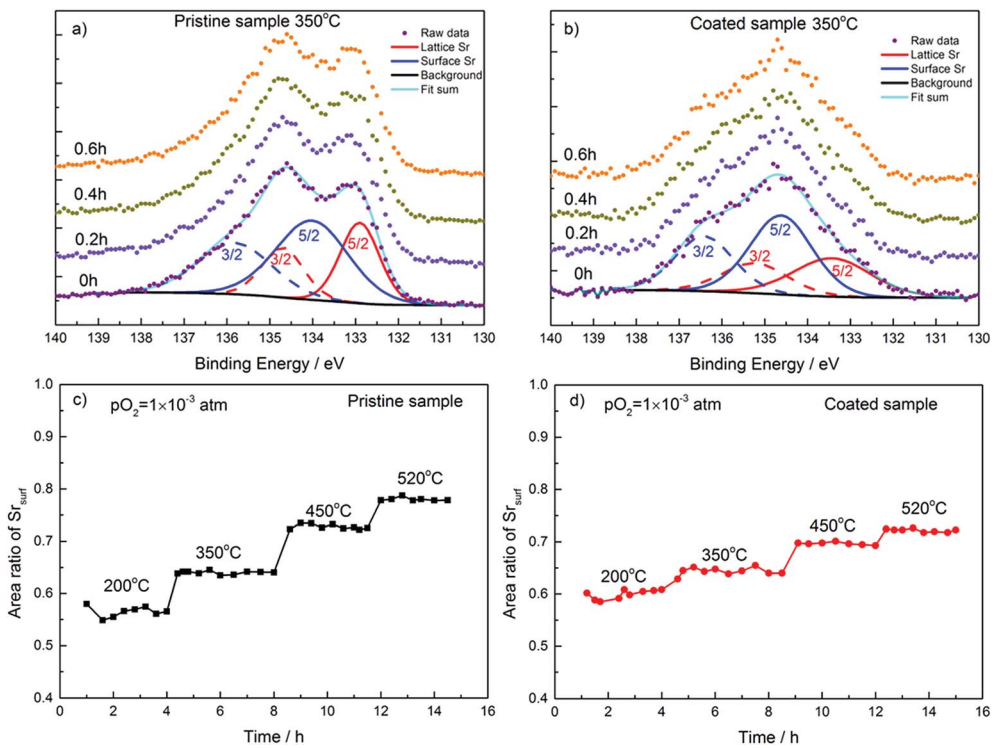

Fig. 3 Time-dependent low-resolution Sr 3d spectra for (a) pristine and (b) coated sample at 350 °C; time-dependent area ratio of surface Sr for (c) pristine and (d) coated sample during the heating process from 200 to 520 °C in an oxygen pressure of 1×10^{-3} atm.

both samples were increasing with the temperature and stabilized as soon as the temperature reached the set point, implying that the surface Sr-segregation process is rather fast. The fast Sr-segregation kinetics was also observed by another study, where the surface Sr-concentration reaching equilibrium was shown within 0.5 h.[18] In a separate ToF-SIMS study, Kubicek *et al.* also observed that Sr-segregation kinetics in the same LSCo epitaxial film on YSZ-single crystal as this study is very fast at 600 °C because of the enhanced chemical diffusion coefficient of Sr, instead of tracer self-diffusion coefficient, by the mobile oxygen vacancy during the ambipolar transport.[30]

Temperature-dependent surface Sr-content. To attain a more accurate analysis of the chemical state in the near surface region of the LSCo thin films, high-resolution Sr 3d and O 1s spectra of another group of pristine and coated LSCo films were collected and the results are shown in Fig. 4 and 5 as a function of temperature. The peak positions at different temperatures were calibrated with the La 4d spectra as well. The O 1s spectra were divided into 3 sets that can be associated with lattice Sr, SrO and absorbed –(OH) with the binding energy of 534.3, 535.6 and 537.0 eV, respectively.[31,32] The binding energies (BE), full-width-half-maximum (fwhm), and peak area for each component of the high-resolution scans are listed in Tables S1 and S2 of the ESI.† The La 4d, Co 3p and Zr 3d spectra are also shown in Fig. S2 of the ESI† for reference.

For the pristine sample, Fig. 4b shows that the content (area ratio) of lattice Sr is less than the surface Sr at RT; however, at 250 °C the content of lattice Sr increases drastically, which could be due to the removal of the carbon-containing species on the surface. As the temperature is further increased to 350 °C, the content of surface Sr shows a significant increase, suggesting the onset of Sr segregation as similarly reported in other work.[13] From 350 to 520 °C, the content of surface Sr continues to increase, and it is worth noticing that the peak position of surface Sr continues to shift towards higher binding energy. Although the surface components were described as one set of Sr $3d_{5/2}$ and $3d_{3/2}$ doublets in many early studies on chemical state in the near-surface region of LSCo films,[18,27,33] there could be more than one species such as SrO and $Sr(OH)_2$. Due to the close Sr peak position of SrO with other surface components, we cannot obtain a precise quantification analysis from Sr spectra. But the existence of $Sr(OH)_2$ at lower temperature and its decomposition at higher temperatures would explain the energy shift and thus give a better description of the surface compositions at different temperatures. The maximum surface Sr content at 520 °C is 76% of the total Sr in the near-surface region for the pristine sample.

For the O 1s spectra of the pristine sample, Fig. 4c shows the same trend as Sr. At RT, the peak at around 537 eV is much higher than the other two peaks, indicating a large amount of surface contaminations. As the temperature is raised to 250 °C when the contaminations are quickly removed, the content of lattice oxygen is increased in the same way as Sr. From 250 to 520 °C, the oxygen in SrO keeps increasing and finally becomes the dominant component, making the lattice oxygen less pronounced. The oxygen peak of –(OH) starts to fade at 350 °C and finally disappears at 520 °C, corresponding to the decomposition of $Sr(OH)_2$. Overall, the Sr 3d and O 1s spectra show a clear evidence of Sr segregation and variations of surface compositions with temperature in the pristine sample.

The Sr 3d and O 1s spectra of the ALD-coated sample are shown in Fig. 5. In general, Fig. 5b shows that Sr 3d peak intensities of the coated sample are much lower that of the pristine sample. At RT, one can still see the same 2 sets of Sr-spectral components. At 250 °C, the intensity of both surface Sr and lattice Sr peaks become stronger because of the removal of surface carbon species. From 250 to 520 °C, the surface Sr keeps increasing while the lattice Sr keeps decreasing. The peak position of surface Sr remains unchanged, suggesting the surface component on the coated sample is mainly SrO. This is different from what was observed on the pristine sample, implying that the ALD process (at 180 °C) may remove some surface species. At 520 °C, the content of surface Sr components is ~75%, which is similar to that of pristine sample. But the actual amount of surface Sr components should be presented by a proper quantification analysis, which will be discussed later.

The O 1s spectra for the ALD-coated sample shown in Fig. 5c are more complicated. At RT, there seems to be 4 sets of spectral peaks: 530.5 eV for the lattice O, 531.8 eV for O associated with surface Sr, 531.2 eV and 532.1 eV for lattice O associated with Zr,[34] and 533.4 eV for surface carbon species. As the temperature is raised to 250 °C, the peak at 533.4 eV disappears, confirming the removal of carbon species. While from 250 to 520 °C, a clear trend of changes in surface and lattice O cannot be observed because those O peaks are too close to discern; a small shift of binding energy in the analysis could lead to a significant difference and make it very hard to produce reliable results. However, since the O 1s peak of the coated sample can be well fitted with 4 sets of oxygen peaks, it can still be considered as a good indicator of the existence of surface and lattice Sr components, which makes the analysis for Sr-chemistry valid.

Equilibrium surface Sr concentration *vs.* temperature. Due to the existence of ZrO_2 layer on the surface of the coated sample, the surface-to-lattice Sr-ratio cannot fairly represent the degree of surface Sr-segregation in both the pristine and coated samples. So, the atomic fraction of La, Sr, Co, O and Zr (denoted as [La], $[Sr]_{tot}$, [Co], [O] and [Zr], respectively) were calculated based on their normalized intensities that were obtained by normalizing the peak area with photoionized cross-section and inelastic mean free path of each elements (see Table S3 of the ESI†); this is a technique that has been used elsewhere.[27,35] The results from 250 to 520 °C (RT data was not included due to the adsorbed carbon-containing species) are shown in Fig. 6a and b, where the atomic fraction of each element is compared for the two samples.

For the pristine sample at RT, $[Sr]_{tot}$ is larger than [La] and [Co] because of the existence of rich surface Sr components. From 250 to 520 °C, $[Sr]_{tot}$ is increased gradually because of the migration of Sr in the bulk towards the near surface region where XPS can detect. For the coated sample, [Zr] and [O] are dominant over the entire temperature range studied; this is because XPS is only sensitive to the near surface region and the thickness of ZrO_2 is close to the probe depth. The ratio of [Co]/[lattice] ([lattice] = [La] + $[Sr]_{lat}$ + [Co]) and $[Sr]_{surf}$/[lattice] for

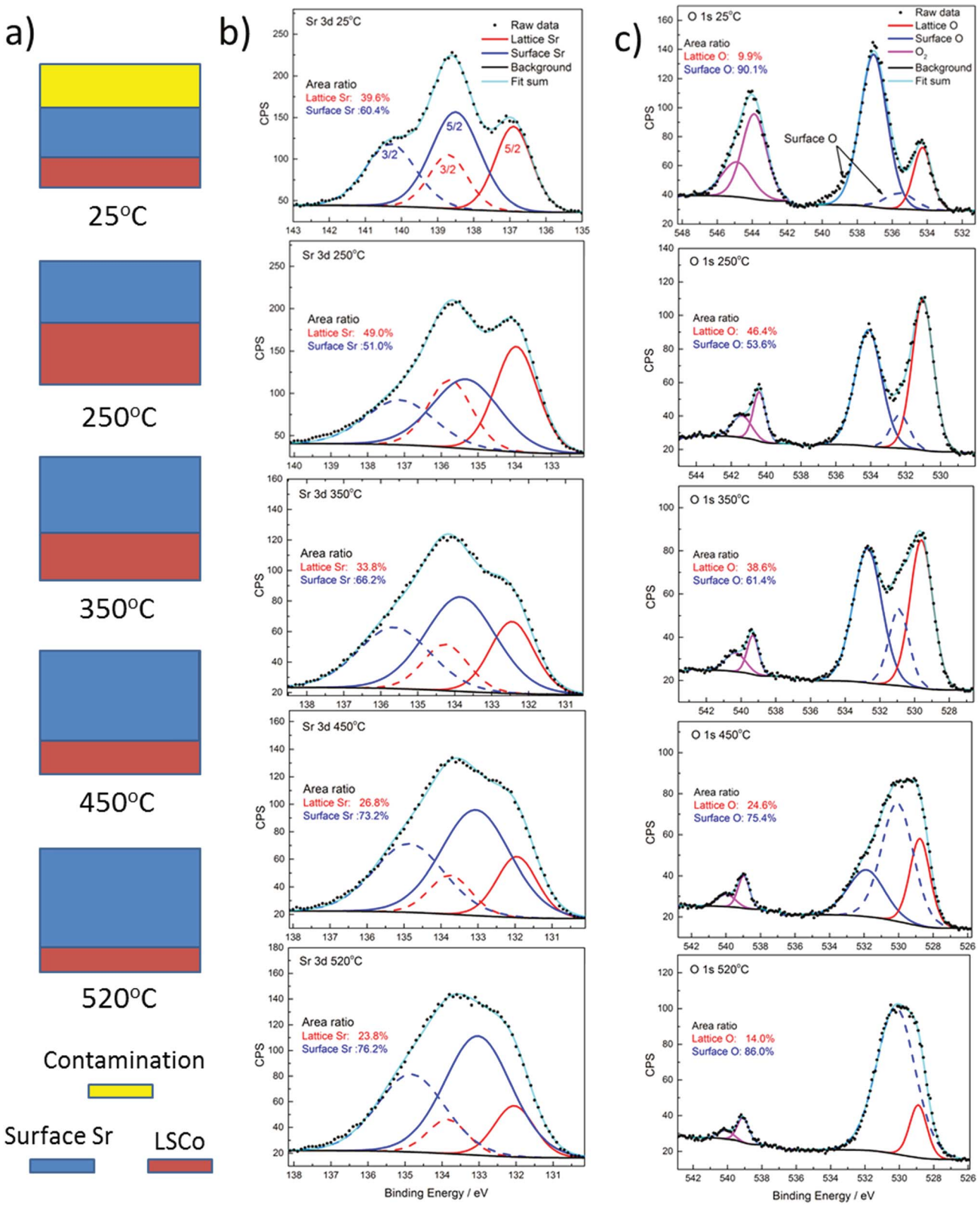

Fig. 4 (a) Schematic of surface states in the pristine sample at different temperatures; (b) Sr 3d and (c) O 1s spectra of the pristine sample at different temperatures in an oxygen pressure of 1×10^{-3} atm.

both samples were calculated and presented in Fig. 6c. The ratio of [Co]/[lattice] for both samples varies from 0.50–0.55, which is close to the stoichiometry of LSCo, despite the increase in temperature and low atomic fractions of La, Sr and Co in the coated sample, indicating the validity of spectral analysis and quantification process. The ratio of $[Sr]_{surf}$/[lattice] for both

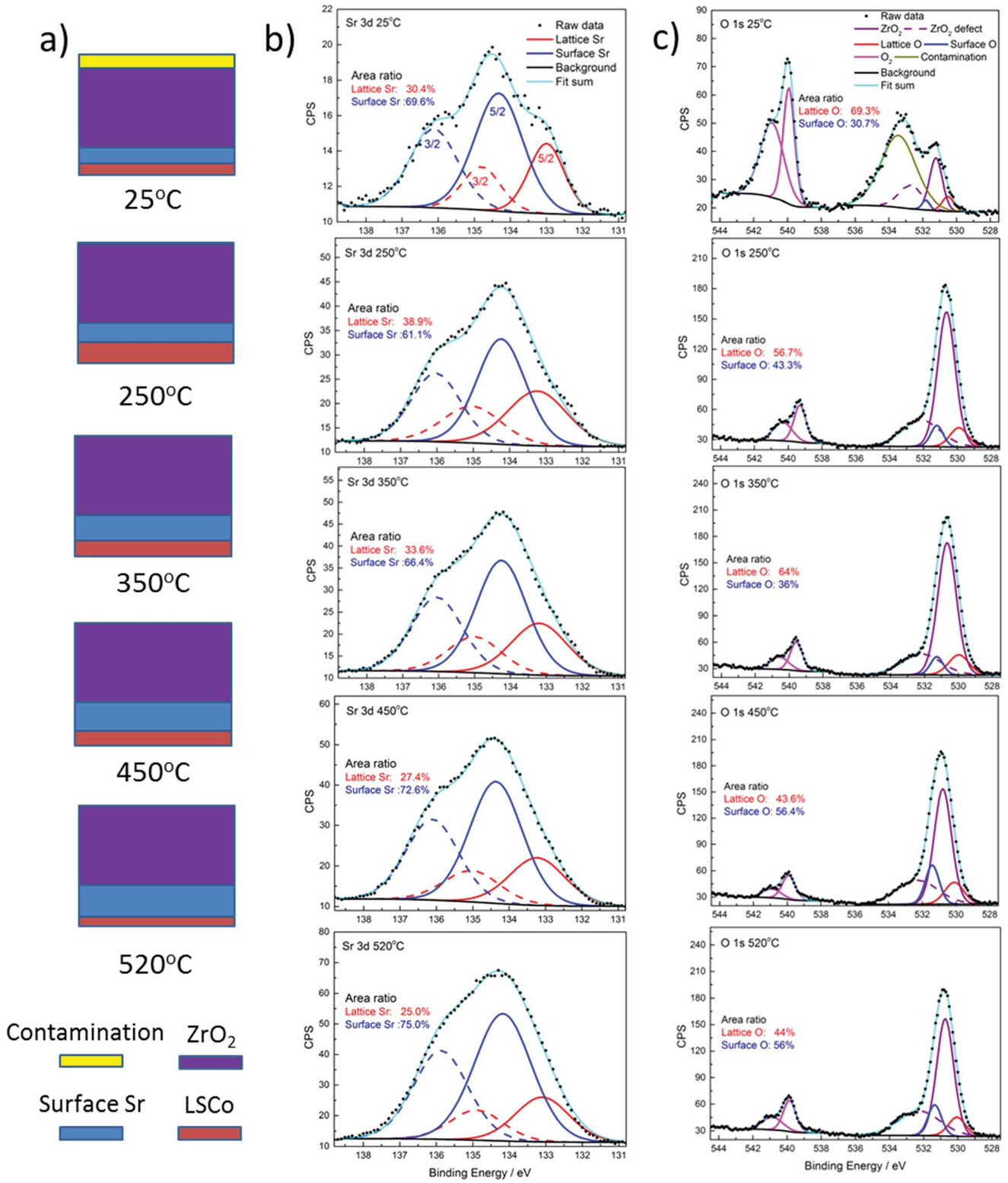

Fig. 5 (a) Schematic of surface states in the ALD-coated sample at different temperatures; (b) Sr 3d and (c) O 1s spectra of the coated sample at different temperatures in an oxygen pressure of 1×10^{-3} atm.

samples increases with temperature, but it is obvious that the ratio in the pristine sample increases faster and ends up with a higher value at 520 °C.

To the interest of this study, we present the equilibrium atomic fractions of surface Sr ($[Sr]_{surf}$) of the two samples in Arrhenius format, $\ln([Sr]_{surf})$ *vs.* $1/T$, from 250 to 520 °C in

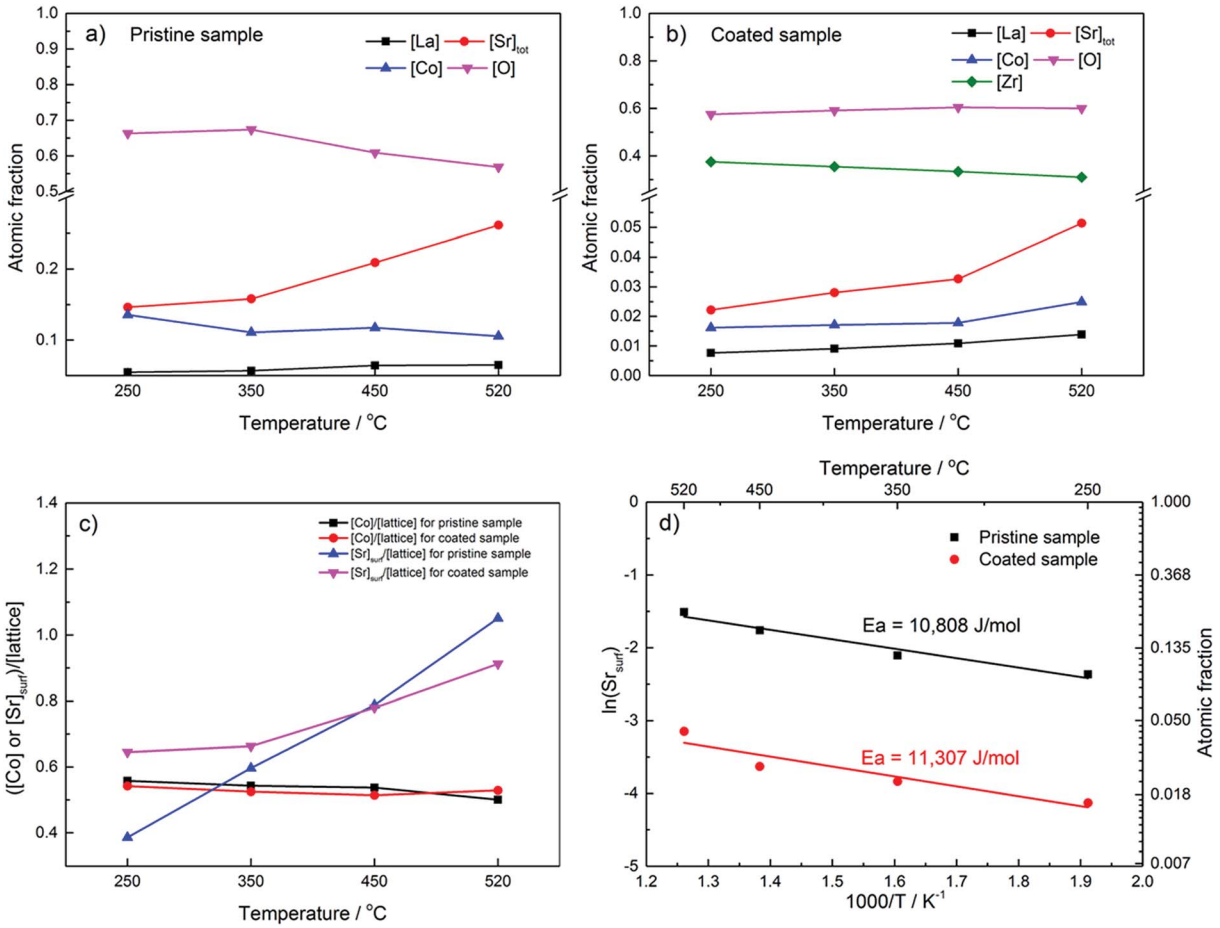

Fig. 6 Temperature-dependent atomic concentrations of (a) pristine and (b) ALD-coated samples; (c) temperature-dependent [Co]/[lattice] and $[Sr]_{surf}$/[lattice] ratio; (d) Arrhenius plots of atomic fractions of surface Sr in both samples.

Fig. 6d. It is evident that $[Sr]_{surf}$ of both samples increases from 250 to 520 °C, and $[Sr]_{surf}$ of the coated sample is much smaller than that of the pristine sample (~4% *vs.* ~22% at 520 °C). The plots in Fig. 6d is found to follow the Arrhenius relationships:

For the pristine sample:

$$[Sr_{surf}] = 1.06 \exp\left(-\frac{10808}{RT}\right) \quad (1)$$

For the coated sample:

$$[Sr_{surf}] = 0.205 \exp\left(-\frac{11307}{RT}\right) \quad (2)$$

where, R is the gas constant, 8.314 J mol^{-1} K^{-1}; T is absolute temperature, K. The activation energy E_a (J mol^{-1}) for the coated sample is a slightly higher than that of the pristine sample, implying that it is a little more difficult for Sr to migrate to the surface in the coated sample than in the pristine sample. The major determining factor is the pre-exponential factor for the two samples. However, the overall magnitude of E_a is much smaller than other similar thermally-activated process such as Sr diffusion in $SrTiO_3$ (~372 kJ mol^{-1})[36] or Mg segregation in Al–Mg alloy (64 kJ mol^{-1}),[37] suggesting that the Sr-segregation in LSCo is an easy diffusion process that does not need significant thermal energy to activate. This finding is also supported by another study.[30]

The presence of high concentration of surface oxygen vacancies in the pristine LSCo is the driving force for the easy Sr-segregation. For the coated LSCo, the Zr-substitution on the Co-site near the surface region creates positive charged defect $Zr^{\bullet}_{Co}$, thus decreasing $[V^{\bullet\bullet}_{O}]$ on the surface as required by the local charge neutrality, and thus the electrostatic attraction to pull the negatively charged Sr-defect (Sr'_{La}) towards the surface. The present study supports this hypothesis rather than "strain-effect" hypothesis because the thin-film HRXRD results did not reveal any strains in the thin films with or without ZrO_2 overcoat.

3.4 EIS analysis

The time-dependent EIS measurements were performed to characterize the thermal stability of the pristine and coated LSCo films using the impedance cell shown in Fig. S1.† The EIS spectra are shown in Fig. 7a with the equivalent circuit as the inset for fitting R_o and R_p; R_o is the highest-frequency intercept with the Z'-axis, representing the ohmic resistance; R_p is the length between highest and lowest frequency on the Z'-axis,

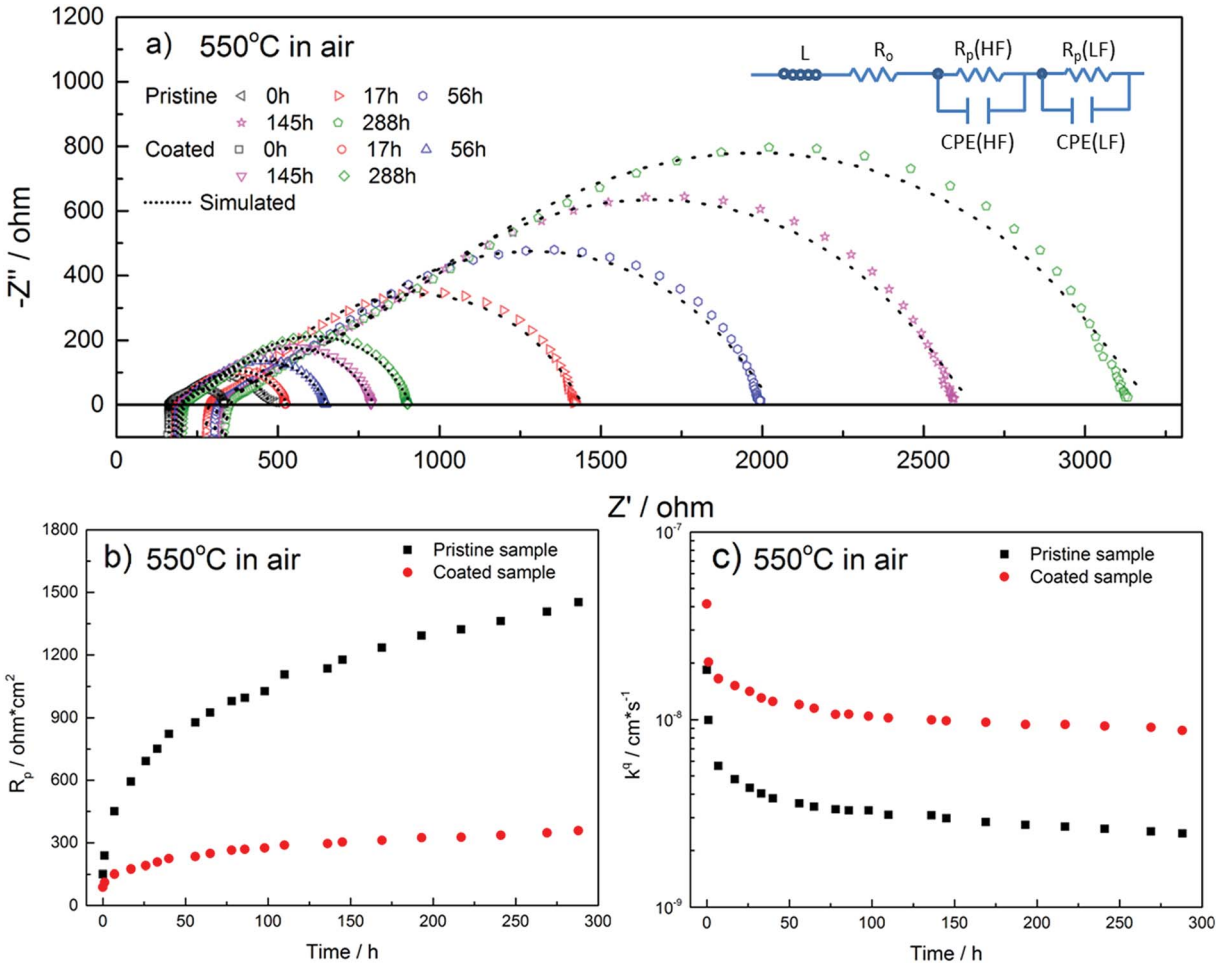

Fig. 7 (a) Comparison of Nyquist plots of pristine and coated samples for select time intervals, inset is the equivalent electrical circuit for EIS spectra simulation; (b) time-dependent R_p values and (c) surface oxygen exchange coefficients *vs.* time of the pristine and coated samples measured at 550 °C in ambient air.

representing the polarization resistance. The obtained R_p values for the two samples are compared in Fig. 7b for 300 h. From the beginning, R_p of the pristine sample was larger than that of the coated one. From APXPS data, we know that the pristine sample already has a large $[Sr]_{surf}$ at 520 °C, which is responsible for the higher R_p. As the time elapses, R_p of the pristine sample grows precipitously with time at a rate of 4.3 ohm cm^2 h^{-1}; for the coated sample, the R_p increases at a much smaller rate of 0.9 ohm cm^2 h^{-1}, further demonstrating of beneficial effect of ALD-ZrO_2 coating in suppressing Sr-segregation and thus stabilizing the polarization resistance.

The low-frequency $R_{p(LF)}$ is associated with the oxygen adsorption/dissociation process, *i.e.* surface oxygen exchange process,[38,39] and can be used to calculate the surface exchange coefficient k^q by:[40]

$$k^q = \frac{RT}{4F^2 R_{p(LF)} A c_0} \quad (3)$$

where R and T have their usual meanings; F is the Faraday's constant; A is the electrode area; c_0 is the lattice oxygen concentration in LSCo, 0.089 mol cm^{-3} in this study.[33] The k^q of the coated sample is in reasonable range of the reported value,[23,25] and about 2× higher than that of pristine sample at the beginning of the test and 4× higher at 300 h marker. For the thin film sample, there is no structural complexity, meaning that such difference should not be attributed to geometrical effects, but to the true chemical state in the near-surface region. Therefore, a much stable R_p of the coated samples is another strong evidence of the suppressed Sr segregation by the ZrO_2 layer, consistent with the APXPS results. It is to be noted that R_p values of the thin-film samples are much higher than practical three-dimensional porous electrodes due to the limited reactive areas.

4. Conclusions

In summary, the oxygen-deficient LSCo epitaxial films fabricated by PLD exhibit the desirable (001) normal and (202) off-normal crystallographic orientations with and without ALD-ZrO_2 overcoat. There is no in-plane and out-of-plane strains in the LSCo thin film imposed by the ALD-ZrO_2-overcoat from the relaxed lattice parameter analysis. The Sr bulk-to-surface

segregation of pristine and ALD-ZrO_2-overcoated LSCo epitaxial films investigated by *in situ* APXPS as a function of time and temperature at a fixed oxygen partial pressure of 1×10^{-3} atm show fast kinetics, but the amount of surface Sr in the coated sample is significantly lower than that of the pristine sample. The equilibrium surface Sr concentration is found to follow Arrhenius relationship, but with a small activation energy, suggesting that Sr bulk-to-surface migration is a weak thermally-activated diffusion process. The concentration-dependent pre-exponential term plays a major role in the Sr-segregation process. The suppressed Sr surface migration in the coated film is resulted from the cation exchange between Zr and Co near the sub-surface region, thus reducing surface $[V_O^{\bullet\bullet}]$ and the electrostatic force to pull Sr-defect (Sr'_{La}) to the surface. Correspondingly, EIS study reveals that the coated sample exhibits a more stable and higher ORR activity than the pristine sample at 550 °C in ambient air over 300 h. Overall, it is concluded that the ALD-ZrO_2 thin layer is effective in suppressing bulk-to-surface Sr segregation in oxygen-vacancy-rich Sr-doped perovskites and thus improving their thermal and electrochemical stability as a cathode for IT-SOFCs.

Conflicts of interest

There are no conflicts to declare.

Acknowledgements

This work is supported by National Science Foundation (NSF) under award NSF-DMR-1464112. We would like to thank Dr Yi Yu and Jun Cai in Lawrence Berkeley National Laboratory for the assistance with APXPS, and Kang-Deuk Choi in Park Systems for the assistance with AFM. This research used resources of the Advanced Light Source, which is a DOE Office of Science User Facility under contract no. DE-AC02-05CH11231. This research also used resources of PLD thin film deposition at Oak Ridge National Laboratory supported by the U.S. Department of Energy (DOE), Office of Science, Basic Energy Sciences, Materials Science and Engineering Division.

References

1 J. Mizusaki, J. Tabuchi, T. Matsuura, S. Yamauchi and K. Fueki, *J. Electrochem. Soc.*, 1989, **136**, 2082–2088.
2 D. Ding, X. Li, S. Y. Lai, K. Gerdes and M. Liu, *Energy Environ. Sci.*, 2014, **7**, 552–575.
3 A. Egger, E. Bucher, M. Yang and W. Sitte, *Solid State Ionics*, 2012, **225**, 55–60.
4 A. N. Petrov, O. F. Kononchuk, A. V. Andreev, V. A. Cherepanov and P. Kofstad, *Solid State Ionics*, 1995, **80**, 189–199.
5 S. Jiang and J. Love, *Solid State Ionics*, 2001, **138**, 183–190.
6 P. Hjalmarsson, M. Søgaard and M. Mogensen, *Solid State Ionics*, 2008, **179**, 1422–1426.
7 Y. Yu, H. Luo, D. Cetin, X. Lin, K. Ludwig, U. Pal, S. Gopalan and S. Basu, *Appl. Surf. Sci.*, 2014, **323**, 71–77.
8 M. Kubicek, A. Limbeck, T. Frömling, H. Hutter and J. Fleig, *J. Electrochem. Soc.*, 2011, **158**, B727–B734.
9 R. Bertacco, J. Contour, A. Barthélemy and J. Olivier, *Surf. Sci.*, 2002, **511**, 366–372.
10 Y. Chen, W. Jung, Z. Cai, J. J. Kim, H. L. Tuller and B. Yildiz, *Energy Environ. Sci.*, 2012, **5**, 7979–7988.
11 M. Finsterbusch, A. Lussier, J. Schaefer and Y. Idzerda, *Solid State Ionics*, 2012, **212**, 77–80.
12 W. Lee, J. W. Han, Y. Chen, Z. Cai and B. Yildiz, *J. Am. Chem. Soc.*, 2013, **135**, 7909–7925.
13 W. Jung and H. L. Tuller, *Energy Environ. Sci.*, 2012, **5**, 5370–5378.
14 H. B. Lee, F. B. Prinz and W. Cai, *Acta Mater.*, 2010, **58**, 2197–2206.
15 T. T. Fister, D. D. Fong, J. A. Eastman, P. M. Baldo, M. J. Highland, P. H. Fuoss, K. R. Balasubramaniam, J. C. Meador and P. A. Salvador, *Appl. Phys. Lett.*, 2008, **93**, 151904.
16 R. D. Shannon, *Acta Crystallogr., Sect. A: Cryst. Phys., Diffr., Theor. Gen. Crystallogr.*, 1976, **32**, 751–767.
17 Y. Gong, D. Palacio, X. Song, R. L. Patel, X. Liang, X. Zhao, J. B. Goodenough and K. Huang, *Nano Lett.*, 2013, **13**, 4340–4345.
18 N. Tsvetkov, Q. Lu, L. Sun, E. J. Crumlin and B. Yildiz, *Nat. Mater.*, 2016, **15**, 1010–1016.
19 D. F. Ogletree, H. Bluhm, E. D. Hebenstreit and M. Salmeron, *Nucl. Instrum. Methods Phys. Res., Sect. A*, 2009, **601**, 151–160.
20 Y. L. Yang, A. Jacobson, C. Chen, G. Luo, K. Ross and C. Chu, *Appl. Phys. Lett.*, 2001, **79**, 776–778.
21 A. Mitterdorfer and L. Gauckler, *Solid State Ionics*, 1998, **111**, 185–218.
22 J. Ralph, A. Schoeler and M. Krumpelt, *J. Mater. Sci.*, 2001, **36**, 1161–1172.
23 D. Lee, R. Jacobs, Y. Jee, A. Seo, C. Sohn, A. V. Ievlev, O. S. Ovchinnikova, K. Huang, D. Morgan and H. N. Lee, *J. Phys. Chem. C*, 2017, **121**, 25651–25658.
24 D. Lee, Y.-L. Lee, W. T. Hong, M. D. Biegalski, D. Morgan and Y. Shao-Horn, *J. Mater. Chem. A*, 2015, **3**, 2144–2157.
25 E. J. Crumlin, S.-J. Ahn, D. Lee, E. Mutoro, M. D. Biegalski, H. M. Christen and Y. Shao-Horn, *J. Electrochem. Soc.*, 2012, **159**, F219–F225.
26 M. E. Grass, P. G. Karlsson, F. Aksoy, M. Lundqvist, B. Wannberg, B. S. Mun, Z. Hussain and Z. Liu, *Rev. Sci. Instrum.*, 2010, **81**, 053106.
27 E. J. Crumlin, E. Mutoro, Z. Liu, M. E. Grass, M. D. Biegalski, Y.-L. Lee, D. Morgan, H. M. Christen, H. Bluhm and Y. Shao-Horn, *Energy Environ. Sci.*, 2012, **5**, 6081–6088.
28 D. Lee, Y.-L. Lee, A. Grimaud, W. T. Hong, M. D. Biegalski, D. Morgan and Y. Shao-Horn, *J. Phys. Chem. C*, 2014, **118**, 14326–14334.
29 Z. Feng, E. J. Crumlin, W. T. Hong, D. Lee, E. Mutoro, M. D. Biegalski, H. Zhou, H. Bluhm, H. M. Christen and Y. Shao-Horn, *J. Phys. Chem. Lett.*, 2013, **4**, 1512–1518.
30 M. Kubicek, G. M. Rupp, S. Huber, A. Penn, A. K. Opitz, J. Bernardi, M. Stöger-Pollach, H. Hutter and J. Fleig, *Phys. Chem. Chem. Phys.*, 2014, **16**, 2715–2726

31 J.-C. Dupin, D. Gonbeau, P. Vinatier and A. Levasseur, *Phys. Chem. Chem. Phys.*, 2000, **2**, 1319–1324.
32 P. Van Der Heide, *Surf. Interface Anal.*, 2002, **33**, 414–425.
33 E. Mutoro, E. J. Crumlin, M. D. Biegalski, H. M. Christen and Y. Shao-Horn, *Energy Environ. Sci.*, 2011, **4**, 3689–3696.
34 H. Zhai, J. Kong, J. Yang, J. Xu, Q. Xu, H. Sun, A. Li and D. Wu, *J. Mater. Sci. Technol.*, 2016, **32**, 676–680.
35 K. A. Stoerzinger, W. T. Hong, E. J. Crumlin, H. Bluhm, M. D. Biegalski and Y. Shao-Horn, *J. Phys. Chem. C*, 2014, **118**, 19733–19741.
36 K. Gömann, G. Borchardt, M. Schulz, A. Gömann, W. Maus-Friedrichs, B. Lesage, O. Kaïtasov, S. Hoffmann-Eifert and T. Schneller, *Phys. Chem. Chem. Phys.*, 2005, **7**, 2053–2060.
37 S. Saied and J. Sullivan, *J. Phys.: Condens. Matter*, 1993, **5**, A165.
38 Y. L. Yang, A. Jacobson, C. Chen, G. Luo, K. Ross and C. Chu, *Appl. Phys. Lett.*, 2001, **79**, 776–778.
39 Y. Yang, C. Chen, S. Chen, C. Chu and A. Jacobson, *J. Electrochem. Soc.*, 2000, **147**, 4001–4007.
40 F. S. Baumann, J. Fleig, H.-U. Habermeier and J. Maier, *Solid State Ionics*, 2006, **177**, 1071–1081.